# Supporting Information

## Cook et al. 10.1073/pnas.0810200106

### SI Text

We forced all of our model simulations with observed SSTs from the Hadley Center analysis (1). The inability of the GISS model to generate a realistic Dust Bowl drought from SST forcing alone is not a unique quality of the GISS model. Other modeling studies using different models and different SST forcing datasets have had similar difficulty, even as they are able to reproduce other examples of SST forced drought (e.g., refs. 2–5). The GISS model replicates the climate of the 20th Century when forced with modern forcings and observed SSTs, including low- and high-frequency variability and trends (6). Using the simulations from ref. 6, we have plotted the North American drought of the 1950s, compared against observations (Fig. S1). In the case of the 1950s drought, land degradation and dust aerosols are thought to be unimportant. With SST forcing only, the GISS model produces the main features (spatial extent, intensity) of this drought. This, together with the simulation results of of other models, reinforces the notion that poor simulation the Dust Bowl drought in our SST-ONLY runs is due to missing physical processes (i.e., the missing land surface factors) and not some underlying model deficiency.

**Dust Emissions and Crop Failure.** Few quantitative estimates of wind erosion, dust source magnitude, or dust aerosol loading for the Dust Bowl era are available. Source area is somewhat better constrained, and we based our placement of the dust source in the SST+DUST and the SST+DUST+CROP experiments on the erosion map from ref. 7 (Fig. 2). Based on this map, we placed a highly productive dust source (3 times the maximum default dust sources in the GISS ModelE) over the model region 106.25E–93.75E and 33N–49N. Annual dust emission, deposition, and net emission (emission − deposition) from this source area for both dust experiments and each ensemble member are shown in Fig. S2. For comparison, it is estimated that wind erosion accounted for soil losses from the Great Plains of 350 million metric tons in 1934 (8) and 770 million metric tons in 1935 (7). If we compare this against our net emissions (Emission − Deposition) over our dust source area, our simulations yield fluxes of comparable magnitude. Ensemble average net emissions in the SST+DUST scenario are 395 million metric tons during 1934 and 340 million metric tons during 1935. Average annual emissions across the ensemble for 1932–1939 are 369 million metric tons per year. For SST+DUST+CROP the results are similar: net emissions of 442 and 337 million metric tons for 1934 and 1935, respectively, and an average loss of 374 million metric tons per year. In light of the admittedly uncertain observational estimates, our modeled dust emissions match closely to available observations. In fact, for 1935 (and possibly other years for which data are unavailable), it appears we err on the side of underestimating the dust emissions and subsequent aerosol forcing.

Our devegetated area (Fig. 2 from main article), designed to mimic the crop failure during the period, was slightly larger than the region over which we added the dust source: 108.75E–93.75E and 31N–49N. Again, there are few spatial estimates of crop failure during the period, although evidence suggests quite high and significant abandonment of agricultural lands and loss of vegetation cover during the period (7). Our crop failure area was expanded compared with the dust source area to account for areas in the map that experienced significant wind or water erosion rather than just wind erosion. We took water erosion to be indicative of loss of vegetation cover without being a dust aerosol source because the soil was eroded by water rather than the wind. We limited our devegetated area to crops, assuming no loss of natural vegetation during the drought. Much like our dust source, we view this as a "conservative" estimate and believe we are likely to actually underestimate the boundary forcing due to vegetation loss.

**Mechanisms.** Whereas the precipitation anomalies originate in forcing from SST anomalies, both the temperature and precipitation anomalies in our model experiments are subsequently modified through surface feedbacks, because the loss of vegetation and dust aerosol loading alters the energy balance at the surface and the fluxes of latent and sensible heating. Figs. S3–S6 show differences between the various model experiments (for the period 1932–1939) and a control run with SST forcing only (SST-ONLY, 1932–1939). This is designed to show the added effect of dust or vegetation loss on top of the forcing from SSTs.

In the SST+CROP case, the major model response in these experiments is an increase in surface temperature. The warming associated with the crop failure is centered over the northern Great Plains. During the summer period (June–July–August), the loss of vegetation through the conversion of crops to bare soil sharply reduces evapotranspiration by severely reducing the transpiration component (fluxes of water through plants while the plants are actively photosynthesizing) of the surface water flux. The surface energy balance during the summer consequently shifts from latent to sensible heating (Fig. S3), leading to increases in near-surface temperature. Summer warming is carried over into the fall and winter seasons in the form of soil temperature anomalies, which subsequently release heat during the fall and winter seasons (Fig. S4). Both processes (shift from latent to sensible heating during the summer and heat release from soil during the winter) are present and active in the SST+DUST+CROP experiments, but their impact is partially countered due to the cooling effect of the dust aerosols.

In the SST+DUST and SST+DUST+CROP cases, the dominant effect of the mineral dust aerosols is to reflect incoming solar radiation, reducing the net radiation at the surface and the top of the atmosphere (Fig. S5). To balance, a compensatory increase in atmospheric energy input is required, manifesting as low-level divergence and upper-level convergence, reflected in geopotential height anomalies at 850 hPa, 500 hPa, and 300 hPa (Fig. S6). This leads to a reduction in moisture convergence over the Great Plains and a reduction in precipitation when dust effects are included.

1. Rayner N, et al. (2003) Global analyses of sea surface temperature, sea ice, and night marine air temperature since the late nineteenth century. *J Geophys Res* 108:4407–4443.
2. Herweijer C, Seager R, Cook E (2006) North American droughts of the mid to late nineteenth century: A history, simulation and implication for Mediaeval drought. *Holocene* 16:159–171.
3. Schubert S, Suarez M, Pegion P, Koster R, Bacmeister J (2004) On the cause of the 1930s Dust Bowl. *Science* 303:1855–1859.
4. Seager R, Kushnir Y, Herweijer C, Naik N, Velez J (2005) Modeling of tropical forcing of persistent droughts and pluvials over western North America: 1856–2000. *J Clim* 18:4065–4088.
5. Seager R, et al. (2008) Would advance knowledge of 1930s SSTs have allowed prediction of the Dust Bowl drought? *J Clim* 21:3261–3281.
6. Hansen J, et al. (2007) Climate simulations for 1880 2003 with GISS modelE. *Clim Dyn* 29:661–696.
7. Hansen ZK, Libecap GD (2004) Small farms, externalities, and the Dust Bowl of the 1930s. *J Polit Econ* 112:665–694.
8. Fye FK, Stahle DW, Cook ER (2003) Paleoclimate analogs to Twentieth-Century moisture regimes across the United States. *Bull Am Meteorol Soc* 84:901–909.

**Fig. S1.** Precipitation anomalies for the 1950s drought: observations from the CRU2.1 dataset (*Left*) and modeled anomalies from 20th Century GISS ModelE run (*Right*).

# Great Plains Dust Emissions: SST+DUST Ensemble

**Dust Emissions, million metric tons**

**Dust Deposition, million metric tons**

**Emission−Deposition, million metric tons**



# Great Plains Dust Emissions: SST+DUST+CROP Ensemble

**Dust Emissions, million metric tons**

**Dust Deposition, million metric tons**

**Emission−Deposition, million metric tons**



**Fig. S2.** Annual dust emissions from our Great Plains dust source, for each year and ensemble member from experiments SST+DUST and SST+DUST+CROP. Labels EJ1–EJ5 refer to the individual ensemble members.

**Fig. S3.** Difference in sensible (*Upper*) and latent heating (*Lower*) for the June–July–August period (SST+CROP minus SST-Only). Reductions in vegetated area from crop removal reduce transpiration and total surface water fluxes, shifting the surface energy balance to favor sensible over latent heating.

**Fig. S4.** Difference (SST+CROP − SST-Only) in temperature of the top soil layer for June–August (JJA, *Top*), September–February (SONDJF, *Middle*), and difference in soil heat flux for September–February (SONDJF, *Bottom*). Negative soil heat flux values indicates an anomalous heat flux directed from the soil to the atmosphere.

## Net Radiation, TOA (W m$^{-2}$), SST+DUST minus SST Only



## Net Surface Radiation, (W m$^{-2}$), SST+DUST minus SST Only



**Fig. S5.** Difference in annual net radiation at the top of the atmosphere and at the surface (SST+DUST − SST-Only).
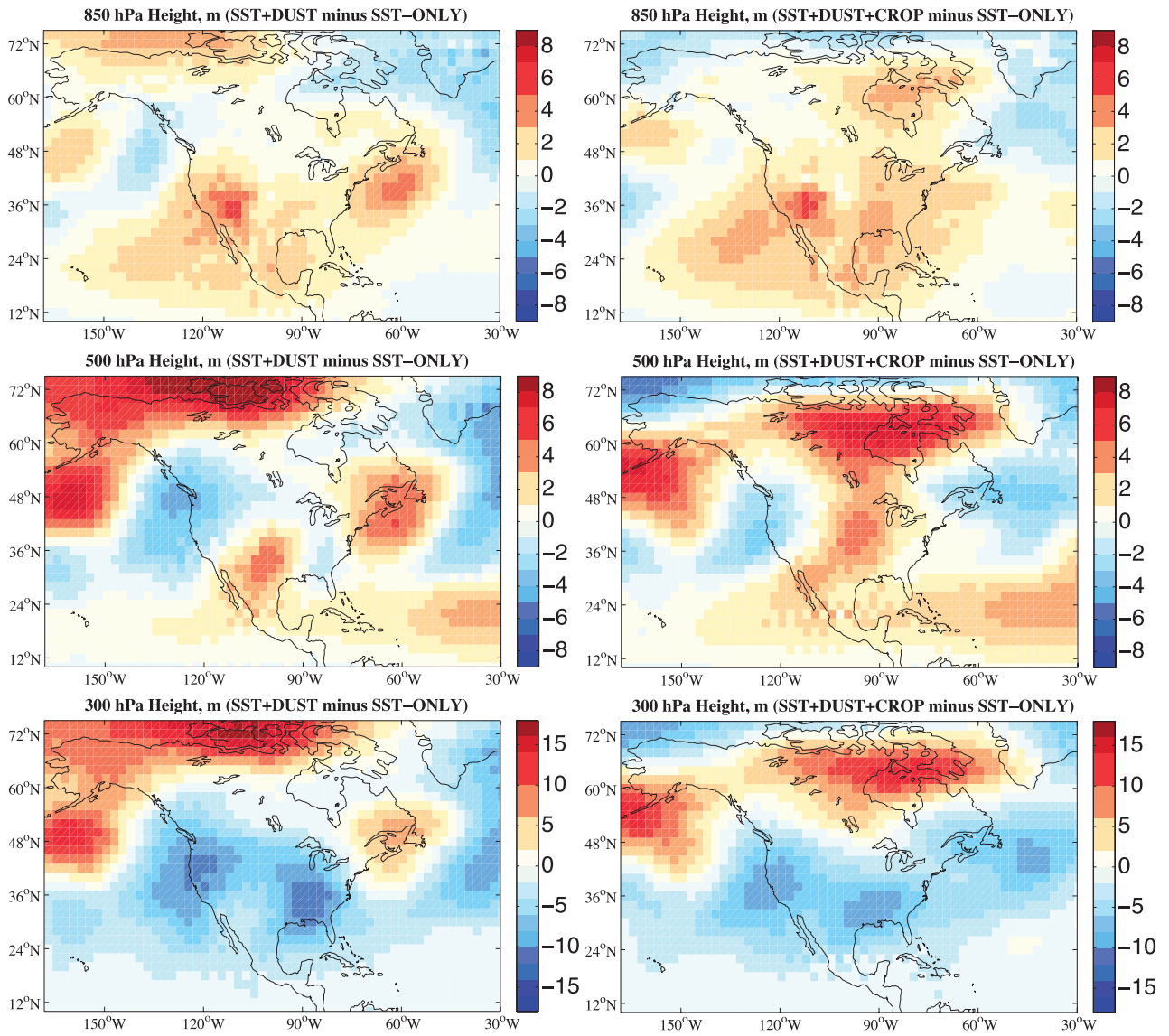
**Fig. S6.** Difference in geopotential heights at 850 hPa, 500 hPa, and 300 hPa (meters, SST+DUST − SST-Only and SST+DUST+CROP − SST-Only).